Analog de Sitter universe in quantum Hall systems with an expanding edge

Yasusada Nambu [1,*] and Masahiro Hotta[2,†]

[1]*Department of Physics, Graduate School of Science, Nagoya University,*
Chikusa, Nagoya 464-8602, Japan
[2]*Department of Physics, Tohoku University, Sendai 980-8578, Japan*

Expanding edges in quantum Hall systems can become a simulator of quantum $1 + 1$ dimensional expanding universes. In these systems, edge excitations are represented as a chiral scalar field in curved spacetimes. We investigate Hawking radiation and entanglement behavior predicted by this model assuming that the expansion law of the edge region corresponds to a de Sitter universe. As observable quantities for the quantum field, local spatial modes associated with detection regions are introduced using window functions for the field, and their correlations are evaluated. We found the impact of Hawking radiation caused by the edge expansion on autocorrelation functions of the local modes, and confirmed that entanglement death due to Hawking radiation occurs. This behavior of entanglement is related to "quantum to classical transition" in cosmic inflations.

I. INTRODUCTION

Analog models of gravitational systems are useful to understand the physics of black holes and early universe [1]. Indeed, although quantum aspects of black hole evaporation with Hawking radiation has been paid much attention theoretically, it is difficult to observe the phenomena in our universe due to its too low temperature for astrophysical black holes. Concerning cosmological particle creations, it is hard to observe the occurrence of this effect in the early stage of the universe directly. However, considering condensed matter systems, it is possible to design models with causal horizons for excitations, which have similar properties as black hole horizons or cosmological horizons for null rays in general relativity. Thus it is possible to perform experiments of analog Hawking radiation [2,3] and particle creations in expanding universes in laboratories. Quantum Hall (QH) systems can become one of such analog models [4–6]. A QH system emerges when a strong perpendicular magnetic field is applied to two-dimensional electrons when the Landau level filling factor becomes an integer or a rational fraction [7,8]. The QH systems are typical topological materials consisting of the bulk and edge. In the bulk, the dynamics yields a large energy gap in its dispersion relation. In the edge, the dispersion relation of the edge current is protected owing to the topological structure of the system, and the edge excitations are always gapless. Thus the edge effective theories

are given by free field theories with a chiral condition, and belong to a class of conformal field theory in $1 + 1$ dimensional spacetime.

Most of all experiments of QH systems have been performed in a static situation. The electrons are confined in the bulk region by a static electric field created by the surface potential of host semiconductors of the 2D electrons and the edge attached to the bulk remains unchanged in time. Expanding edges were proposed in [9] and experimental realization is ongoing [10,11]; the edge expands by gradually relaxing the external electric fields through continuous electron supply into the bulk and the excitations moving along the edge are affected by the expansion. Thus, it is possible to perform experiments of the quantum scalar field in an analog expanding universe. In our previous paper [12], we formulated a quantum field theory in $1 + 1$ dimensional curved spacetime to analyze the edge dynamics. It was shown that the expanding edges can be regarded as expanding universe simulators of two-dimensional dilaton-gravity models, and pointed out that our theoretical setup can simulate the classical counterpart of an analog Hawking radiation with Gibbons-Hawking temperature from the future de Sitter horizon formed in the expanding edge region.

In this paper, applying the formulation developed in our previous paper [12], we investigate quantum aspects of the scalar field in an expanding edge model which reproduces an analog de Sitter universe. In particular, we focus on particle creation in the analog de Sitter universe (Hawking radiation), generation of quantum fluctuations by edge expansion, and their entanglement behavior. We will show that the thermal radiation with the Gibbons-Hawking temperature from the

*[*]nambu@gravity.phys.nagoya-u.ac.jp
[†]hotta@tuhep.phys.tohoku.ac.jp

expanding edge region is created and that it is detectable in a static edge region. For this purpose, instead of introducing a specific detector model to measure the Hawking radiation, we define local spatial modes of the scalar field using window functions and consider their correlations. Further-more, we will also investigate the entanglement between two spatial regions and show that it decreases by Hawking radiation coming from the expanding edge region. We regard this behavior as a feature corresponding to the disappearance of quantumness of the primordial quantum fluctuations expected in cosmic inflations [13–15]. Thus, our analog de Sitter model can be available as a simulator of the early universe to explore the generation mechanism and the feature of primordial quantum fluctuations originated by cosmic inflations.

The plan of the paper is as follows. In Sec. II, we review our setup of the expanding edge of the QH systems and an analog de Sitter universe. In Sec. III, we present the behavior of classical wave propagation in the expanding edge system. In Sec. IV, we formulate the quantum treat-ment of edge excitations and investigate the behavior of spatial local modes which are measurable in an experiment of the QH system. In Sec. V, we discuss entanglement between spatial modes. Section VI is devoted to summary and speculation.

II. EXPANDING EDGE OF QUANTUM HALL SYSTEM

Let us consider a massless scalar field φ on the edge of QH systems. Based on the effective theory of the edge excitations in QH systems [7,8], the edge mode is repre-sented by a massless scalar field φ the wavelength of which is 100 times larger than the magnetic length

$$\ell_B = \sqrt{\frac{\hbar}{eB}}, \qquad (1)$$

where B is a perpendicular magnetic field. The edge current and the edge charge density are given as derivatives of the scalar field. We derive the wave equation for φ. The left moving modes and the right moving modes of φ obey

$$\partial_\tau \varphi_L - \frac{v}{a(\tau)} \partial_x \varphi_L = 0, \qquad \partial_\tau \varphi_R + \frac{v}{a(\tau)} \partial_x \varphi_R = 0, \qquad (2)$$

where τ denotes a time variable in a laboratory, x is the comoving coordinate along the edge and the proper length along the edge is given by $a(\tau) \int dx$. The scale factor $a(\tau)$ represents the expansion of the edge. Using the trapping potential $U(y)$ perpendicular to the edges of the QH system, the propagation speed of the edge excitation v is determined as

$$v = \frac{cU'(y)}{eB} = \frac{cE}{B}, \qquad (3)$$

where E is the electric field induced by U. This propa-gation speed of the edge excitation is the same as the classical drift velocity of electrons. The solution of these equations is

$$\varphi_L = A\left(v\int \frac{d\tau}{a} + x\right), \qquad \varphi_R = B\left(v\int \frac{d\tau}{a} - x\right), \qquad (4)$$

where A, B are arbitrary functions. The scalar field $\varphi := \varphi_L + \varphi_R$ obeys

$$\ddot{\varphi} + \frac{\dot{a}}{a}\dot{\varphi} - \frac{v^2}{a^2}\partial_x^2 \varphi = 0, \qquad \dot{\ } = \frac{\partial}{\partial \tau}. \qquad (5)$$

This is the Klein-Gordon equation $\Box\varphi = 0$ in a $1+1$ dimensional expanding universe, the metric of which is given by

$$ds^2 = -v^2 d\tau^2 + a^2(\tau)dx^2. \qquad (6)$$

The propagation speed of the edge excitation v plays the same role as the speed of light c in general relativity which determines causal structures of spacetimes. It is possible to control the expansion law $a(\tau)$ by tuning the external trapping electric field for the edge region. We can perform experiments of quantum physics of an early universe using the analog expanding universe by analyz-ing QH systems with an expanding edge. From now on, we set $v = 1$ and we use v as a unit of length and time in our analog spacetimes. By introducing the conformal time $t := \int d\tau/a$ and null coordinates $x^\pm := t \pm x$, the metric is written as the conformally flat form:

$$ds^2 = -a^2 dx^+ dx^-. \qquad (7)$$

The scalar field is represented as

$$\varphi = \varphi_L(x^+) + \varphi_R(x^-). \qquad (8)$$

For a given form of $a(\tau)$ which represents the expansion law of the edge region, it is possible to identify a corresponding analog universe using the metric (7). In the QH systems, either φ_L or φ_R is allowed due to the boundary condition of QH systems.

In this paper, we consider an analog de Sitter universe in our setup of the QH system. The left panel of Fig. 1 depicts a setup of our QH experiment with the expanding edge of the QH system: the edge system is composed of an input static region I ($L/2 < x$), an expanding region II ($-L/2 \leq x \leq L/2$), and a output static region III ($x < -L/2$). The analog metric of this system is written as
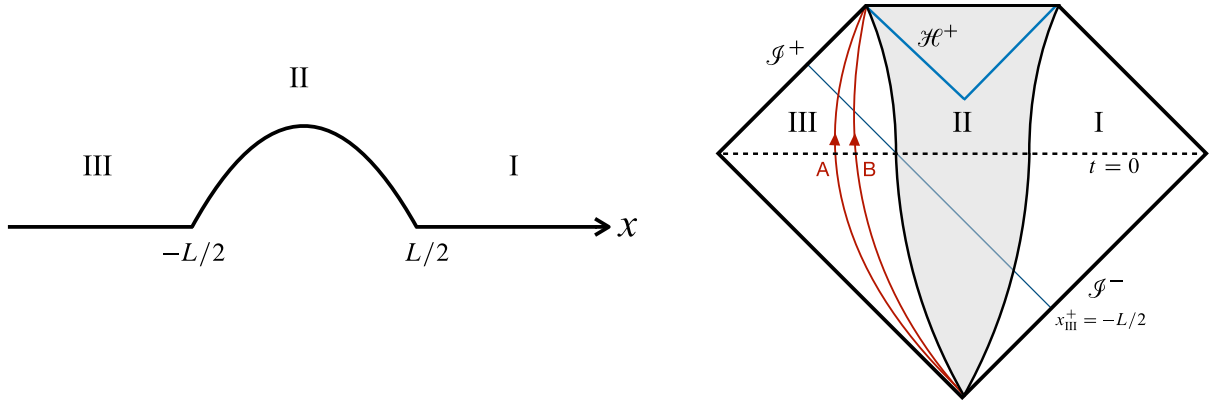
FIG. 1. Left: schematic picture of the expanding edge system. x denotes a coordinate along the edge of the QH system. Regions I and III are static Minkowski regions and the expanding region II corresponds to a de Sitter universe. Right panel: Penrose diagram representing the present setup with the expanding edge region II (gray region), which starts accelerated expansion at $t = 0$. A and B denote world lines of detectors which perform measurements of edge excitations. This diagram corresponds to the $\pi/4 < LH < \pi/2$ case. For parameter values not included in this range, global structure of the spacetime becomes different (see [12]).

$$ds^2 = a^2(t)(-dt^2 + dx^2),$$

$$a(t) = \begin{cases} \frac{1}{\cos(Ht)}\theta(t) + \theta(-t) & \text{for } -L/2 \leq x \leq L/2 \text{ (region II)}, \\ 1 & \text{for } L/2 < |x| \text{ (region I, III)}, \end{cases} \tag{9}$$

where $\theta(t)$ is the Heaviside function. Using the proper time $\tau = \int_0^t dt' a(t')$, the metric in region II is

$$ds^2 = \begin{cases} -d\tau^2 + \cosh^2(H\tau)dx^2, & \text{for } \tau \geq 0. \\ -d\tau^2 + dx^2, & \text{for } \tau < 0. \end{cases} \tag{10}$$

Thus, we assume a spacetime that is flat Minkowski for $t < 0$ and de Sitter expansion starts at $t = 0$ in region II. The global structure of this spacetime is shown in the right panel of Fig. 1 with the parameter $\pi/4 < LH < \pi/2$. There emerges formation of the future de Sitter horizon $\mathcal{H}^+$ in region II. It is possible to obtain a relation between spatial coordinates of regions I and II explicitly. Null coordinates

in regions I and III are related by the following formula (see detail in Appendix A):

$$x_{\mathrm{I}}^+ = \Phi[-L + \Phi^{-1}[x_{\mathrm{III}}^+ + \Phi[L/2]]] + L/2 =: f(x_{\mathrm{III}}^+), \tag{11}$$

$$x_{\mathrm{III}}^- = \Phi[-L + \Phi^{-1}[x_{\mathrm{I}}^- + L/2]] - \Phi[L/2] + L, \tag{12}$$

where the function Φ is defined by Fig. 2

$$\begin{aligned} \Phi(x) &= \int_0^x dy\, a(y) \\ &= \begin{cases} \frac{1}{2H} \ln \frac{1+\sin Hx}{1-\sin Hx} & \text{for } 0 \leq x < \frac{\pi}{2H}, \\ x & \text{for } x < 0. \end{cases} \end{aligned} \tag{13}$$

The inverse function is

$$\Phi^{-1}(x) = \begin{cases} \frac{1}{H} \arcsin \tanh(Hx) & \text{for } x > 0 \\ x & \text{for } x < 0, \end{cases} \tag{14}$$
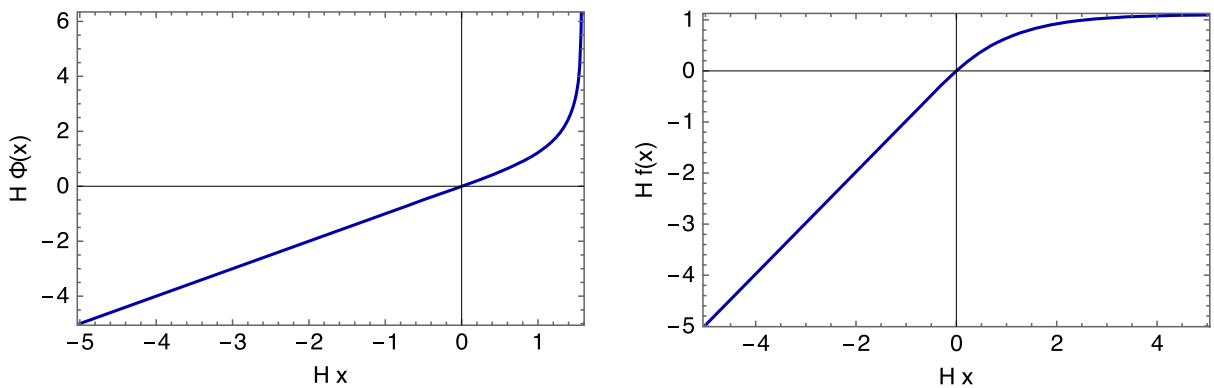

FIG. 2. Left panel: the function $\Phi(x)$. $\Phi = +\infty$ at $Hx = \pi/2$. Right panel: the function $f(x)$.

and for $x \to +\infty$,

$$\Phi^{-1}(x) \sim \frac{\pi}{2H} - \frac{2}{H} e^{-Hx}. \tag{15}$$

The asymptotic form of the function $f(x_{\text{III}}^+) = x_{\text{I}}^+[x_{\text{III}}^+]$ is

$$f(x_{\text{III}}^+) \sim \begin{cases} c_0 - c_1 e^{-Hx_{\text{III}}^+} & \text{for } x_{\text{III}}^+ \to +\infty \\ x_{\text{III}}^+ & \text{for } x_{\text{III}}^+ \to -\infty, \end{cases} \tag{16}$$

where the constants c_0 and c_1 are

$$c_0 = \frac{L}{2} - \ln \tan(HL/2),$$

$$c_1 = \frac{2}{H \sin HL} \sqrt{\frac{1 - \sin HL/2}{1 + \sin HL/2}}. \tag{17}$$

III. CLASSICAL SIMULATION OF HAWKING RADIATION

We send plane waves from region I (in-region) and detect them at a point in region III (out-region). Normalized wave modes in regions I and III are

$$\varphi_k^{(\text{I})} = \frac{e^{-ikx_{\text{I}}^+}}{\sqrt{4\pi k}} = \frac{e^{-ikf(x_{\text{III}}^+)}}{\sqrt{4\pi k}}, \quad \varphi_k^{(\text{III})} = \frac{e^{-ikx_{\text{III}}^+}}{\sqrt{4\pi k}}, \quad k > 0. \tag{18}$$

An input plane wave $e^{-ikx_{\text{I}}^+}$ in region I has the wave form $\exp(-ikf(x_{\text{III}}^+))$ in region III. Distortion of plane waves due to de Sitter expansion of region II is encoded in the function $f(x_{\text{III}}^+)$. Figure 3 depicts wave forms in region III. The left panel shows the real part and the imaginary part of $\varphi_k^{(\text{I})}$ as the function of x_{III}^+. The right panel shows snapshots of wave forms $\text{Re}\varphi_k^{(\text{I})}$ at $t = 0, 3, 6$. We can observe the wave is stretched by de Sitter expansion in region II.
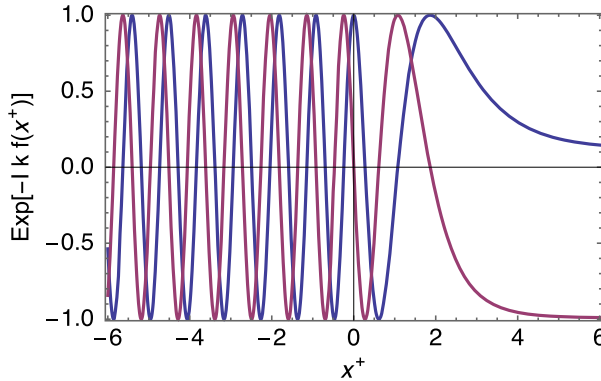
The in-mode and out-mode are related by the Bogoliubov transformation,

$$\varphi_k^{(\text{I})} = \int_0^\infty dk' \left[\alpha(k, k')\varphi_{k'}^{(\text{III})} + \beta(k, k')\varphi_{k'}^{(\text{III})*} \right], \tag{19}$$

$$\varphi_k^{(\text{III})} = \int_0^\infty dk' \left[\alpha^*(k', k)\varphi_{k'}^{(\text{I})} - \beta(k', k)\varphi_{k'}^{(\text{I})*} \right], \tag{20}$$

where Bogoliubov coefficients α and β are obtained from the relation

$$\frac{e^{-ik'f(x_{\text{III}}^+)}}{\sqrt{k'}} = \int_0^\infty \frac{dk}{\sqrt{k}} \left[\alpha(k, k')e^{-ikx_{\text{III}}^+} + \beta(k, k')e^{ikx_{\text{III}}^+} \right]. \tag{21}$$

Thus,

$$\alpha(k, k') = \frac{1}{2\pi} \sqrt{\frac{k}{k'}} \int_{-\infty}^\infty dy\, e^{-ik'f(y)} e^{iky},$$

$$\beta(k, k') = \frac{1}{2\pi} \sqrt{\frac{k}{k'}} \int_{-\infty}^\infty dy\, e^{-ik'f(y)} e^{-iky}. \tag{22}$$

Using the asymptotic form (16) of $f(x)$, we have [12]

$$|\beta(k, k')|^2 \sim \begin{cases} 0 & \text{for } x_{\text{III}}^+ \to -\infty, \\ \frac{1}{2\pi Hk'} \frac{1}{\exp(2\pi k/H) - 1} & \text{for } x_{\text{III}}^+ \to +\infty. \end{cases} \tag{23}$$

For $x_{\text{III}}^+ \to +\infty$, the Bogoliubov coefficient β shows the Planckian distribution with a temperature

$$T_H = \frac{H}{2\pi}. \tag{24}$$

This temperature coincides with the Gibbons-Hawking temperature in the de Sitter spacetime. Thus, it is possible to detect the classical counterpart of Hawking radiation from the cosmological horizon in a de Sitter universe by
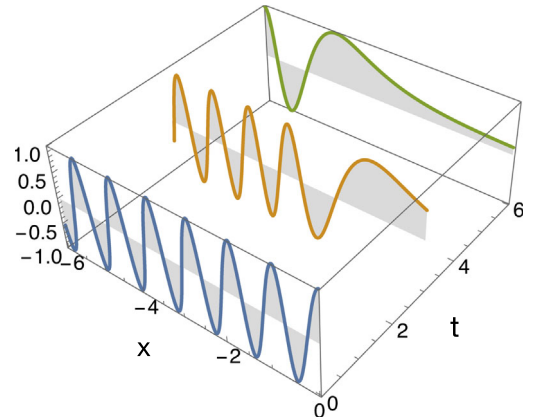

FIG. 3. Wave forms in region III ($L = H = 1, k = 7$). Left panel: real part (blue) and imaginary part (red) of φ. Right panel: change of the spatial profile of waves (real part of φ) at different times ($t = 0, 3, 6$).

measuring the Fourier component of wave signals in the Minkowski region III.

IV. QUANTUM SIMULATION OF HAWKING RADIATION

From now on, we consider a quantum scalar field $\hat{\varphi}$ in the expanding edge system. Our main purpose is to investigate quantum effects of the edge mode in the quantum Hall system, which is measurable through the local charge density $\partial_{x^+}\hat{\varphi}$ of the edge excitation.

A. Correlation functions

Let us consider the setup shown in Fig. 1. We prepare measurement points A and B in region III. At these points, a part of the signals emitted from $\mathscr{I}^-$ of region I cannot reach region III after the formation of the future de Sitter horizon $\mathscr{H}^+$ in region II. Thus, the spacetime structure is similar to that with a black hole formation by gravitational collapse. We consider detection of quantum fluctuations of the scalar field in region III by imposing the vacuum condition at $\mathscr{I}^-$ in region I:

$$\hat{a}_k|0_I\rangle = 0. \tag{25}$$

Owing to the chirality of the edge mode, we only consider a left moving scalar field and the field operator in region III is expressed as

$$\hat{\varphi}(x^+) = \int_0^\infty \frac{dk}{\sqrt{4\pi k}}[\hat{a}_k e^{-ikf(x^+)} + \hat{a}_k^\dagger e^{ikf(x^+)}]. \tag{26}$$

In our setup, the gauge invariant physical quantity is charge density, which is given by the derivative of the field operator $\hat{\varphi}$:

$$\hat{\Pi}(x^+) := \hat{\varphi}'(x^+)$$
$$= -if'(x^+)\int_0^\infty dk\sqrt{\frac{k}{4\pi}}[\hat{a}_k e^{-ikf(x^+)} - \hat{a}_k^\dagger e^{ikf(x^+)}]. \tag{27}$$

We investigate quantum effects based on the field operator $\hat{\Pi}$. Commutators between field operators are

$$[\hat{\varphi}(x^+), \hat{\varphi}(y^+)] = -\frac{i}{4}\text{sign}(f(x^+) - f(y^+)), \tag{28}$$

$$[\hat{\varphi}(x^+), \hat{\Pi}(y^+)] = \frac{i}{2}f'(y^+)\delta(f(x^+) - f(y^+)), \tag{29}$$

$$[\hat{\Pi}(x^+), \hat{\Pi}(y^+)] = \frac{i}{2}f'(x^+)f'(y^+)\delta'(f(x^+) - f(y^+)). \tag{30}$$

The Wightman function for $\hat{\varphi}$ is

$$D(x_1^+, x_2^+) = \langle \hat{\varphi}(x_1^+)\hat{\varphi}(x_2^+)\rangle$$
$$= \frac{1}{4\pi}\int_\mu^\infty \frac{dk}{k}e^{-ik(f(x_1^+)-f(x_2^+)-i\Delta f)}$$
$$= -\frac{1}{4\pi}\log[\mu(f(x_1^+) - f(x_2^+) - i\Delta f)], \tag{31}$$

where we introduced an IR cutoff μ as the lower bound of the integral, and a UV cutoff $\Delta f > 0$ by

$$\Delta f := f'((x_1^+ + x_2^+)/2)|_{x_1^+=x_2^+}\epsilon, \tag{32}$$

with the spatial cutoff length ϵ in the flat region III. In the Minkowski phase $t < 0$, $\Delta f = \epsilon$, and in the de Sitter phase $t \geq 0$, $\Delta f \sim e^{-Ht}\epsilon$ which corresponds to the comoving wavelength in the de Sitter region II. The local spatial modes prepared in the Minkowski region III can detect long wavelength quantum fluctuation in the de Sitter region II. In our analysis, the scalar field $\hat{\varphi}$ is an effective one and there exists the short-distance cutoff length ϵ below which effective treatment of the edge mode breaks down. In the QH systems, this scale corresponds to the magnetic length ℓ_B. We regard the short-distance cutoff ϵ as this length in our analysis.

The Wightman function for $\hat{\Pi}$ is

$$D_\Pi(x_1^+, x_2^+) := \langle \hat{\Pi}(x_1^+)\hat{\Pi}(x_2^+)\rangle = \partial_{x_1^+}\partial_{x_2^+}D(x_1^+, x_2^+)$$
$$= \frac{f'(x_1^+)f'(x_2^+)}{4\pi}\int_0^\infty dkk e^{-ik(f(x_1^+)-f(x_2^+)-i\Delta f)}$$
$$= -\frac{1}{4\pi}\frac{f'(x_1^+)f'(x_2^+)}{(f(x_1^+) - f(x_2^+) - i\Delta f)^2}. \tag{33}$$

This quantity is independent of the IR cutoff μ. Using (16), the asymptotic behavior becomes

$$D_\Pi(x_1^+, x_2^+)$$
$$\sim -\frac{1}{4\pi}\begin{cases} \frac{1}{[(2/H)\sinh(H(x_1^+-x_2^+)/2)-i\epsilon]^2} & \text{for } x_{1,2}^+ \to +\infty \\ \frac{1}{(x_1^+-x_2^+-i\epsilon)^2} & \text{for } x_{1,2}^+ \to -\infty. \end{cases} \tag{34}$$

For $x_1^+, x_2^+ \to +\infty$, D_Π has the same behavior as that of a thermal state with the Gibbons-Hawking temperature T_H. Correlation functions are

$$\langle \{\hat{\varphi}(x^+), \hat{\varphi}(y^+)\}\rangle$$
$$= \frac{1}{2\pi}\int_\mu^\infty \frac{dk}{k}\cos(k(f(x^+) - f(y^+)))e^{-k\Delta f}, \tag{35}$$

$$\langle \{\hat{\varphi}(x^+), \hat{\Pi}(y^+)\} \rangle$$
$$= \frac{f'(y^+)}{2\pi} \int_0^\infty dk \sin(k(f(x^+) - f(y^+)))e^{-k\Delta f}, \quad (36)$$

$$\langle \{\hat{\Pi}(x^+), \hat{\Pi}(y^+)\} \rangle$$
$$= \frac{f'(x^+)f'(y^+)}{2\pi} \int_0^\infty dk\, k \cos(k(f(x^+) - f(y^+)))e^{-k\Delta f}. \quad (37)$$

B. Correlation of local spatial mode

We consider the measurement of the field $\hat{\Pi}(x^+)$ at x_A and x_B in region III. This measurement process can be represented by the interaction between the field operator $\hat{\Pi}$ and the canonical variables $(\hat{Q}_D, \hat{P}_D)$ of the measurement apparatus. In the present analysis, we do not specify details of the apparatus. The interaction Hamiltonian between the field operator and the apparatus is

$$H_{\text{int}} = \sum_{j=A,B} \lambda_j(t)g_j(\hat{Q}_D, \hat{P}_D) \otimes \int dx w_j(x)\hat{\Pi}(t+x), \quad (38)$$

where $g_j(\hat{Q}_D, \hat{P}_D)$ is a function of canonical variables of the measurement apparatus, $w_j(x)$ is a window function defining a spatial local mode of the field at $x_{A,B}$, and $\lambda_j(t)$ is a switching function of the interaction. After acting on the apparatus state, this interaction causes a change of the "reading" of the apparatus depending on the state of the quantum field $\hat{\Pi}$ at $x_{A,B}$. In the present analysis, we do not introduce details of measurement protocols but just pay attention to the behavior of the local mode of the quantum field introduced by the spatial window function $w_{A,B}(x)$.

For the purpose of observing spatial correlations of the field, we define a canonical pair of variables corresponding to the local spatial mode of the field at x_A and x_B:

$$\hat{Q}_j(t) = \int dx w_Q(x - x_j)\hat{\Pi}(t + x),$$

$$\hat{P}_j(t) = \int dx w_P(x - x_j)\hat{\Pi}(t + x), \quad j = A, B. \quad (39)$$

We assume the window functions $w_{P,Q}(x)$ have nonzero values only in a compact spatial region $x \in [-\ell/2, \ell/2]$. Requiring these variables to be canonical pairs, equal time commutators between these variables should be

$$[\hat{Q}_j, \hat{P}_k] = \frac{i}{2} \int dx w_Q(x - x_j)w'_P(x - x_k) \equiv i\delta_{jk}, \quad j, k = A, B, \quad (40)$$

$$[\hat{Q}_j, \hat{Q}_k] = \frac{i}{2} \int dx w_Q(x - x_j)w'_Q(x - x_k) \equiv 0, \quad (41)$$
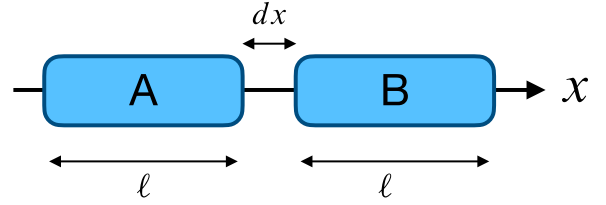

FIG. 4. Setup of defining spatial regions A and B. The center of each region is $x_A = -L/2 - 3\ell/2 - dx$ and $x_B = -L/2 - \ell/2$. $x_B - x_A = \ell + dx$.

$$[\hat{P}_j, \hat{P}_k] = \frac{i}{2} \int dx w_P(x - x_j)w'_P(x - x_k) \equiv 0. \quad (42)$$

These equations provide conditions for window functions and are independent of the state of the quantum field. Thus, the local spatial modes $(\hat{Q}_A, \hat{P}_A)$, $(\hat{Q}_B, \hat{P}_B)$ associated with spatial regions A and B can be introduced by using suitably chosen window functions $w_Q(x)$ and $w_P(x)$ irrespective of the states of the quantum field (Fig. 4). Regions A and B are assumed to have no overlap and their separation is dx. Locality of the spatial modes is guaranteed if we adopt window functions with compact support. The center of each region is assumed to be

$$x_A = -\frac{L}{2} - \frac{3\ell}{2} - dx, \quad x_B = -\frac{L}{2} - \frac{\ell}{2}, \quad x_B - x_A = \ell + dx. \quad (43)$$

We choose the following window functions in our analysis Fig. 5:

$$w_Q(x) = \frac{2}{\sqrt{\pi}} \cos\left(\frac{\pi x}{\ell}\right), \qquad w_P(x) = \frac{2}{\sqrt{\pi}} \sin\left(\frac{\pi x}{\ell}\right),$$
$$x \in [-\ell/2, \ell/2]. \quad (44)$$

These window functions satisfy the condition (40) and the window functions defining the bipartite state for canonical variables $(\hat{Q}_A, \hat{P}_A, \hat{Q}_B, \hat{P}_B)$ do not have spatial overlap for $x_B - x_A \geq \ell$. Equal time correlations of these canonical variables are

$$\langle \hat{Q}_A \hat{Q}_B + \hat{Q}_B \hat{Q}_A \rangle = \int dx dy w_Q(x - x_A)w_Q(y - x_B)$$
$$\times \langle \{\hat{\Pi}(t+x), \hat{\Pi}(t+y)\} \rangle, \quad (45)$$
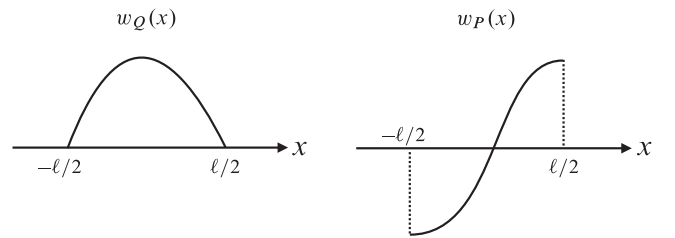

FIG. 5. Spatial profile of adopted window functions.

$$\langle \hat{P}_A \hat{P}_B + \hat{P}_B \hat{P}_A \rangle = \int dx dy w_P(x - x_A) w_P(y - x_B)$$
$$\times \langle \{ \hat{\Pi}(t + x), \hat{\Pi}(t + y) \} \rangle, \qquad (46)$$

$$\langle \hat{Q}_A \hat{P}_B + \hat{P}_B \hat{Q}_A \rangle = \int dx dy w_Q(x - x_A) w_P(y - x_B)$$
$$\times \langle \{ \hat{\Pi}(t + x), \hat{\Pi}(t + y) \} \rangle. \qquad (47)$$

As the bipartite state ρ_{AB} defined by these canonical variables is Gaussian, the state is determined by the covariance matrix

$$V_{AB} = \begin{bmatrix} a_1 & a_3 & c_1 & c_3 \\ a_3 & a_2 & c_4 & c_2 \\ c_1 & c_4 & b_1 & b_3 \\ c_3 & c_2 & b_3 & b_2 \end{bmatrix}, \qquad (48)$$

where its components are defined by

$$c_1 = \frac{1}{2} \langle \hat{Q}_A \hat{Q}_B + \hat{Q}_B \hat{Q}_A \rangle, \qquad c_2 = \frac{1}{2} \langle \hat{P}_A \hat{P}_B + \hat{P}_B \hat{P}_A \rangle,$$
$$c_3 = \frac{1}{2} \langle \hat{Q}_A \hat{P}_B + \hat{P}_B \hat{Q}_A \rangle, \qquad c_4 = \frac{1}{2} \langle \hat{Q}_B \hat{P}_A + \hat{P}_A \hat{Q}_B \rangle,$$
$$\qquad (49)$$

$$a_1 = \langle \hat{Q}_A^2 \rangle, \qquad a_2 = \langle \hat{P}_A^2 \rangle,$$
$$a_3 = \frac{1}{2} \langle \hat{Q}_A \hat{P}_A + \hat{P}_A \hat{Q}_A \rangle, \qquad b_j = a_j(A \to B). \qquad (50)$$

We first show temporal behavior of autocorrelation functions of the local spatial mode in region III. The behavior of the autocorrelation functions $a_{1,2,3}(t)$ with different region size $\ell = 1$, 2 are shown in Fig. 6. We can observe a signature of de Sitter expansion in region II as a change of correlations around $0 < t < 2$. These quantities are measurable as output signals of the detector in our QH experiment. To obtain a qualitative understanding of the behavior of the autocorrelation functions, we evaluate $a_1(t) = \langle \hat{Q}_A^2 \rangle$ analytically with a window function $w_Q(x) = w_0 \theta(\ell/2 + x) \theta(\ell/2 - x)$, where w_0 is a normalization constant the value of which is unspecified:

$$\langle \hat{Q}_A^2 \rangle = \frac{1}{4\pi} \int_0^\infty dk k \left| \int dx w_Q(x) f'(t + x_A + x) e^{ikf(t + x_A + x)} \right|^2 e^{-\Delta f k}$$
$$= \frac{2w_0^2}{\pi} \int_0^\infty \frac{dk}{k} \sin^2 \left[\frac{k}{2} (f(t + x_A + \ell/2) - f(t + x_A - \ell/2)) \right] e^{-\Delta f k}$$
$$= \frac{w_0^2}{4\pi} \ln \left[1 + \frac{(f(t + x_A + \ell/2) - f(t + x_A - \ell/2))^2}{(f'(t + x_A)\epsilon)^2} \right]. \qquad (51)$$

Using the asymptotic form (16) of $f(x)$,

$$\langle \hat{Q}_A^2 \rangle \sim \begin{cases} \frac{w_0^2}{4\pi} \ln[1 + (\frac{\ell}{\epsilon})^2] \approx \frac{w_0^2}{2\pi} \ln(\frac{\ell}{\epsilon}) & \text{for } t \to -\infty, \\ \frac{w_0^2}{4\pi} \ln \left[1 + (\frac{\ell}{\epsilon})^2 \left(\frac{\sinh(H\ell/2)}{(H\ell/2)} \right)^2 \right] \approx \frac{w_0^2}{2\pi} \ln(\frac{\ell}{\epsilon}) + \frac{w_0^2}{2\pi} \ln \left(\frac{\sinh(H\ell/2)}{(H\ell/2)} \right) & \text{for } t \to +\infty, \end{cases} \qquad (52)$$

where we assume that the region size of the detection region is far larger than the UV cutoff and $\ell/\epsilon \gg 1$. The difference of the autocorrelation between $t = -\infty$ and $t = +\infty$ is
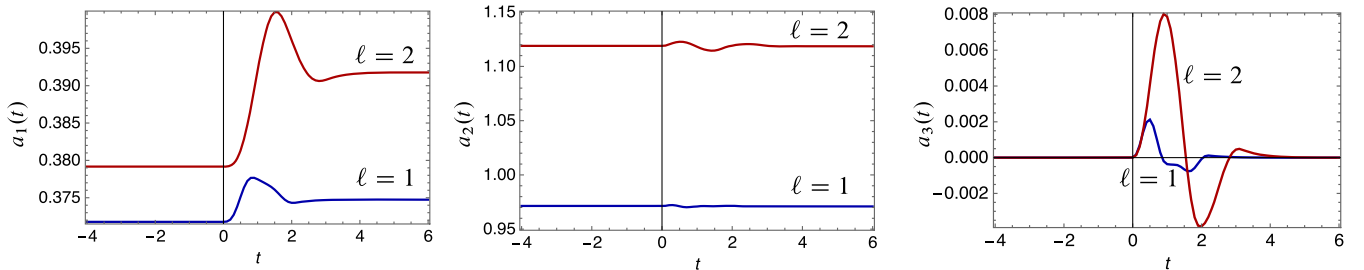

FIG. 6. Behavior of the autocorrelation functions with different region size $\ell = 1$ (blue lines) and $\ell = 2$ (red lines). ($H = L = 1$, $\epsilon = 0.01$).

$$a_1(+\infty) - a_1(-\infty) \sim \frac{w_0^2}{2\pi} \ln\left[\frac{\sinh(H\ell/2)}{(H\ell/2)}\right]. \quad (53)$$

This quantity is independent of the UV cutoff and its amount depends only on $H\ell$. Hence, we expect that it reflects the signature of Hawking radiation from the de Sitter region. For further understanding of the behavior of $a_1 = \langle \hat{Q}_A^2 \rangle$ we pay attention to its ℓ dependence. We expand $a_1(\ell)$ as

$$a_1(\ell) = \int_0^\infty dK \tilde{a}_1(K) e^{iK\ell}. \quad (54)$$

Then, the power spectrum for a_1 is obtained as

$$P(K) = K|\tilde{a}_1(K)|, \quad (55)$$

which represents the power of detected signals with wave number $K = 2\pi/\ell$ corresponding to the size ℓ of the detection region. We see that the power spectrum shows the Planckian distribution with the temperature $T_H = H/(2\pi)$. Using the asymptotic form of a_1 in Eq. (52), the Fourier component of $a_1(\ell)$ is

$$\tilde{a}_1(K) \sim \begin{cases} -\frac{i}{k}(\gamma + \ln(K\epsilon) - i\pi/2) & \text{for } t \to -\infty, \\ \frac{H}{2K^2}[1 - i\frac{2K}{H}(\gamma + \psi(-iK/H))] & \text{for } t \to +\infty, \end{cases} \quad (56)$$

where γ is Euler's constant and $\psi(x) = \Gamma'(x)/\Gamma(x)$ is the poly Gamma function. For $t \to -\infty$, the power spectrum of the signal is

$$P(K) \sim -\ln(K\epsilon). \quad (57)$$

For $t \to +\infty$, the power spectrum of the signal is

$$P(K) \sim \frac{\pi}{e^{2\pi K/H} - 1} \quad \text{for } K < H. \quad (58)$$

Therefore, for long wavelength modes larger than the de Sitter horizon size H^{-1}, the power spectrum observed in region III shows the Planckian distribution with temperature $T_H = H/(2\pi)$ originated from Hawking radiation in the de Sitter region II. Comparing (57) and (58), the power $P(t = +\infty)$ is larger than $P(t = -\infty)$ in the long wavelength region $K < H$ due to the Hawking radiation. This enhancement or amplification of the power for long wavelength fluctuations larger than the de Sitter horizon H^{-1} has the same physical origin as that of the generation of primordial quantum fluctuations in cosmic inflation.

To understand the behavior of Hawking radiation in more detail, we consider the covariance matrix of a single mode $(\hat{Q}_A, \hat{P}_A)$,
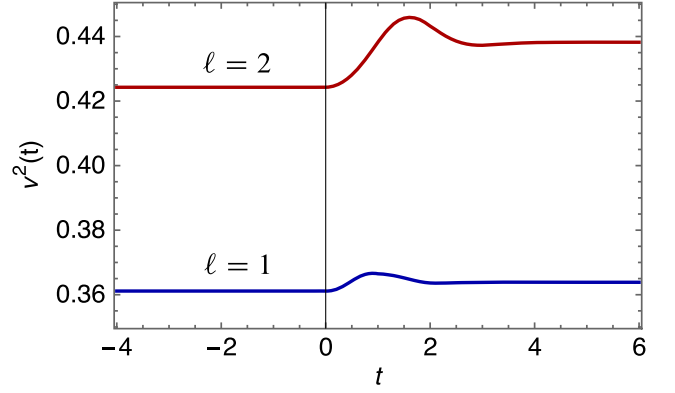

FIG. 7. Evolution of the symplectic eigenvalue of the state ρ_A. $\nu^2 - 1/4$ represents the mixedness of this state, which also represents the amount of entanglement between A and $\bar{A}$.

$$V_A = \begin{bmatrix} a_1 & a_3 \\ a_3 & a_2 \end{bmatrix}, \quad (59)$$

and determinant of this matrix, which is the square of the symplectic eigenvalue ν^2 of the reduced state ρ_A. The physical condition of the state requires $\nu^2 \geq 1/4$ and $\nu^2 = 1/4$ corresponds to a pure state. As we are considering a single subregion A of the entire space, the state ρ_A is mixed and the mixedness represents the amount of entanglement between A and its complement $\bar{A}$. Temporal behavior of ν^2 (Fig. 7) shows Hawking radiation causes an increase of mixedness of the mode A and enhances entanglement between A and $\bar{A}$. The mode A and $\bar{A}$ constitutes a pure two mode squeezed state and its amount of squeezing and entanglement between A and $\bar{A}$ increases due to the Hawking radiation created by the rapid accelerated expansion of the background space.

V. ENTANGLEMENT OF SPATIAL MODES

We investigate behavior of entanglement between spatial regions A and B in region III (Fig. 4) using associated spatial local modes $(\hat{Q}_A, \hat{P}_A)$ and $(\hat{Q}_B, \hat{P}_B)$. We can evaluate entanglement negativity from the symplectic eigenvalues of the covariance matrix V_{AB}; the covariance matrix V_{AB} has two symplectic eigenvalues $\nu_\pm \geq 1/2$, and the partially transposed covariance matrix $\tilde{V}_{AB}$ has two symplectic eigenvalues $\tilde{\nu}_\pm$. Based on the positivity criterion of the partially transposed covariance matrix for bipartite Gaussian states [16–18], a measure of entanglement between A and B is given by the logarithmic negativity defined as [19,20]

$$E_N := -\min[\log_2(2\tilde{\nu}_-), 0]. \quad (60)$$

For $E_N > 0$, the bipartite state ρ_{AB} is entangled and the logarithmic negativity represents the amount of entanglement between A and B.
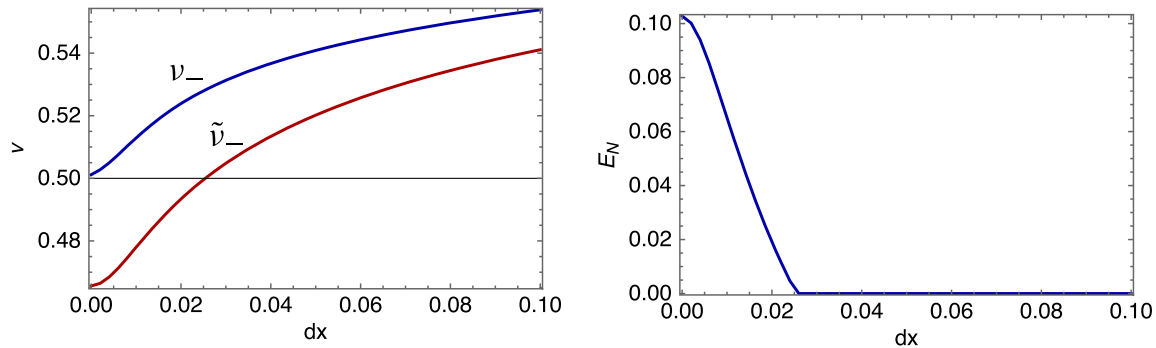
FIG. 8.   Left panel: separation dependence of symplectic eigenvalues ν_-(blue), $\tilde{\nu}_-$(red). Positivity of the bipartite state $\nu_- \geq 1/2$ is preserved for $dx \geq 0$. For $\tilde{\nu}_- < 1/2$, A and B are entangled. Right panel: separation dependence of logarithmic negativity for the Minkowski case. The bipartite state ρ_{AB} becomes separable for large separation ($\epsilon = 0.01$, $\ell = 1$, $L = 1$). The critical separation depends on the values of the UV cutoff ϵ.
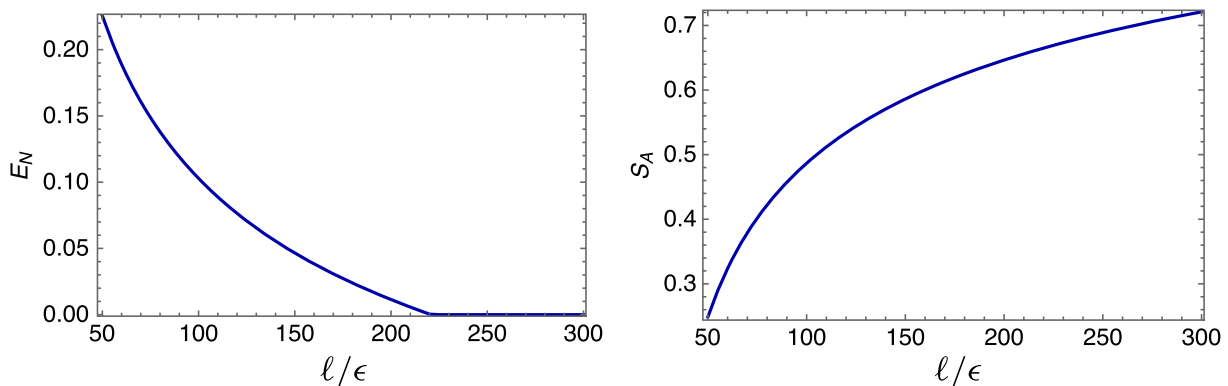

FIG. 9.   Left panel: ℓ/ϵ dependence of negativity with $dx = 0$. Right panel: ℓ/ϵ dependence of entanglement entropy for a single region A. For $\ell/\epsilon \gg 1$, the entanglement entropy behaves as $S_A \propto \log(\ell/\epsilon)$.

A. Minkowski case

We first show the behavior of entanglement for the case that region II is static and there is no expanding edge region (Minkowski case). We confirm that the detection of entanglement between A and B is possible using local modes defined by window functions (44). The left panel of Fig. 8 shows the symplectic eigenvalues as a function of separation dx of two regions, and the right panel of Fig. 8 shows the negativity as a function of dx. There exists a critical separation and below this separation entanglement between A and B can be detected. The left panel of Fig. 9 shows the dependence of the cutoff parameter ℓ/ϵ on negativity with $dx = 0$. For large values of the ratio ℓ/ϵ, the bipartite system AB becomes separable and local modes cannot detect entanglement of the scalar field. It is possible to understand this behavior from the viewpoint of entanglement monogamy [21]. Let us focus on the entanglement entropy of region A which is a subsystem of the entire spatial region. The entanglement entropy for a single Gaussian mode $(\hat{Q}_A, \hat{P}_A)$ is given by [22]

$$S_A = (\nu + 1/2) \log_2(\nu + 1/2) - (\nu - 1/2) \log_2(\nu - 1/2) \tag{61}$$

with the symplectic eigenvalue ν of the covariance matrix V_A for the mode A. As is shown in the right panel of Fig. 9, S_A behaves $\propto \log(\ell/\epsilon)$,[1] which is the typical scaling behavior of entanglement entropy of the massless scalar field in the $1 + 1$ dimensional case [23,24]. This behavior implies that entanglement between region A and its complement becomes larger as ℓ/ϵ increases. Concerning entanglement between A and B, because A and its complement and B and its complement become strongly entangled as ℓ/ϵ becomes larger, owing to the monogamy property of multipartite entanglement [21,25], the entanglement between A and B should become smaller and the entanglement between A and B vanishes above a some critical value of ℓ/ϵ.

B. De Sitter case

We move on to the expanding edge case which mimics a de Sitter universe and consider entanglement between adjacent regions A and B in region III under the influence of Hawking radiation from the de Sitter region II.

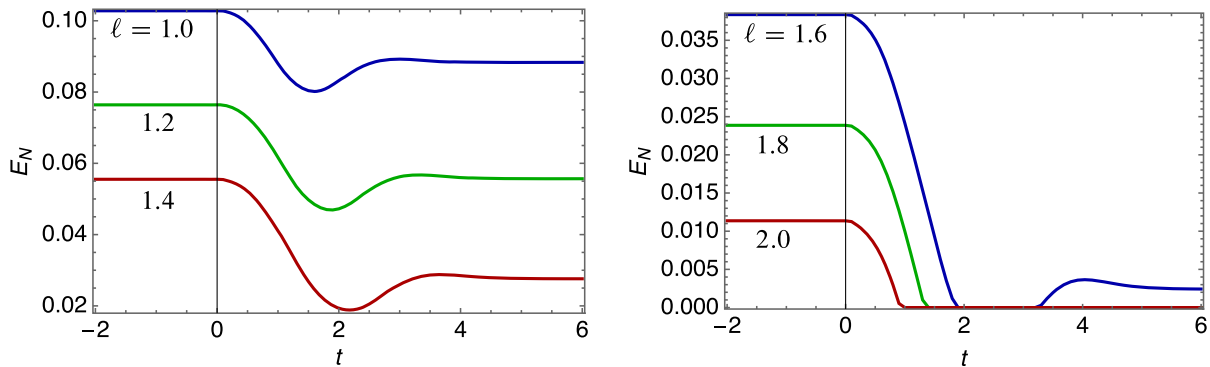[1]This behavior is confirmed numerically and we do not derive this relation analytically.

FIG. 10. Evolution of negativity between regions A and B for the de Sitter case with different spatial region size ℓ ($dx = 0$, $\epsilon = 0.01$, $H = L = 1$). Because of Hawking radiation from the de Sitter region, negativity decreases around $t = 0 \sim 2$. The final value of negativity becomes smaller than the initial negativity in the Minkowski region. For $\ell = 1.8$, 2.0, the final value of negativity becomes zero and entanglement death occurs. For $\ell = 1.6$, both death and revival of entanglement are observed.

Figure 10 shows the evolution of entanglement between A and B with different sizes of A and B with $dx = 0$. As we can observe from Fig. 10, following the transient change of negativity during $0 < t < 3$, which is determined by the shape of the window function, the negativity becomes asymptotically constant. The final amount of entanglement is reduced compared to the initial Minkowski value. The reduction of entanglement depends on the size of spatial regions ℓ. For $\ell = 1.0$–1.4, a nonzero value of negativity survives at $t = 6$. On the other hand, for sufficiently large region size $\ell \gg H^{-1}$, which corresponds to detection of long wavelength superhorizon fluctuation in the de Sitter universe, the entanglement between A and B becomes zero after arrival of the Hawking radiation. This behavior of "entanglement death" is the same as that confirmed in inflationary models [13–15] and is responsible for the emergence of classical behavior from quantum fluctuations. Thus, using our setup of the QH experiment, it is possible to simulate "classical to quantum transition" of primordial quantum fluctuations in a laboratory.

Figure 11 shows the region size dependence of the negativity at $t = 6$. For $\ell \geq 1.65$, the negativity becomes zero and the two regions A and B become separable. The quantum correlation between the two regions is lost for large scales compared to the de Sitter horizon length H^{-1}. For these large scales, spatial correlations between A and B exist as classical correlations. Therefore, the long wavelength Hawking radiation can be treated as classical stochastic fluctuations and we can confirm the classicality of Hawking radiation originated from zero point quantum fluctuations of the scalar field.

VI. SUMMARY AND SPECULATION

We considered the analog de Sitter universe realized by the expanding edge of a QH system. We investigated the behavior of the chiral massless scalar field corresponding to an edge excitation, and discussed the detection of Hawking radiation from the de Sitter region. In our setup of the expanding edge system, the spacetime structure is similar to that of a black hole formation via gravitational collapse; the future event horizon is formed and Hawking radiation with thermal spectrum from the vicinity of the future event horizon is expected. The entanglement between spatial regions A and B in the flat region is also evaluated and we found that Hawking radiation from the de Sitter region reduces preexistent entanglement before the arrival of Hawking radiation, and for sufficient large size of detection regions compared to the Hubble length in the de Sitter region, the two regions become separable and only classical correlation survives. This behavior is the same as that appearing in cosmic inflation. To conduct the UV divergence of the quantum scalar field, we introduced a UV cutoff as the scale at which the effective field treatment of the edge excitation breaks down. The correlation functions of the local spatial modes also contain this cutoff dependence and it is possible to examine the impact of the cutoff on Hawking radiation using our experiment, which is related to the trans-Planckian problem in black hole
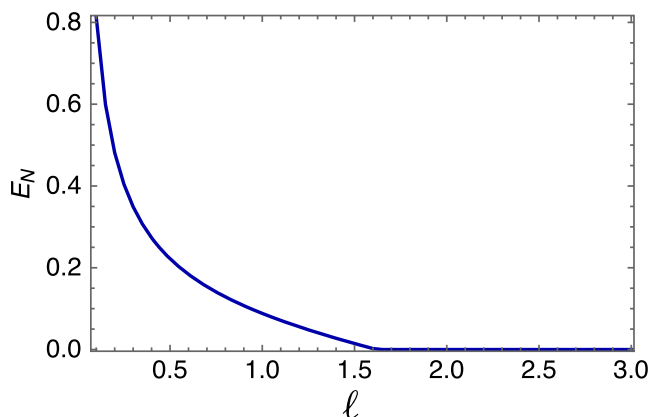

FIG. 11. Region size dependence of negativity at $t = 6$ ($dx = 0$, $L = H = 1$, $\epsilon = 0.01$). A and B become separable for large scales $\ell \geq 1.65 H^{-1}$.

evaporation and cosmic inflations. It is important to investigate how the effective theory for the edge excitation breaks down below the cutoff length since the deviation from the effective theory may introduce corrections to the massless Klein-Gordon equation adopted in this paper. Beside applying the expanding edge of the QH system as a simulator of the quantum cosmology, it is also possible to explore physics of fundamental aspects of quantum mechanics and quantum field theory because this system can provide the squeezed vacuum state by amplification of the vacuum fluctuations in the expanding edge region. Thus, investigation of the violation of macrorealism (the Legget-Garg inequality [26]) with the quantum field and the realization of the quantum energy teleportation [9] are possible.

In this paper, the Hall edges are described by quantum field theory in curved space in the long wavelength regime compared to the magnetic length ℓ_B. As seen in the above analysis, the edge can be regarded as a fixed $1+1$ dimensional universe. It may be interesting to point out a possibility that the same system can be described by different effective theories of quantum gravity. For instance, let us consider a static QH system confined in a circle edge. The edge is regarded as a closed $1+1$ dimensional universe, the spacetime curvature curvature of which vanishes. Since the electrons located at the edge are in a quantum state with position fluctuation, the edge fluctuates quantum mechanically. This yields quantum superposition of edge configurations with different edge lengths. In this sense, quantum universes with different sizes are quantum mechanically superposed. This suggests a realization of quantum gravity at the QH edge. Though the precise model for the static quantum universe has not yet been specified, the classical action may be given by the following dilaton gravity model:

$$S = \int d^2x \sqrt{-g(x)} \left(\Phi(x)R(x) + \frac{\Lambda}{\ell_B} \right), \quad (62)$$

where Λ is a positive constant, $\Phi(x)$ is a real scalar field referred to as dilaton field, and $R(x)$ is the scalar curvature of the $1+1$ dimensional universe. Taking the variation of S with respect to $\Phi(x)$ yields $R(x) = 0$ as the equation of motion. Thus, the classical action is evaluated as

$$S_{QG} = \frac{\Lambda}{\ell_B} \int d^2x \sqrt{-g(x)}. \quad (63)$$

By using a static configuration of φ independent of t, let us parametrize the edge in the $x - y$ plane as

$$(x, y) = (x, \ell_B \varphi(x)), \quad (64)$$

where the edge fluctuation occurs in the y direction. The induced metric for the edge is given by

$$ds^2 = -dt^2 + dx^2 + dy^2 = -dt^2 + h(x)dx^2, \quad (65)$$

where $h(x) = 1 + \ell_B^2(\partial_x\varphi(x))^2$. Then the value of S_{QG} is computed as

$$S_{QG} = \frac{\Lambda}{\ell_B} \int d^2x \sqrt{1 + \ell_B^2(\partial_x\varphi(x))^2}. \quad (66)$$

It may be worth noting that the above value of S_{QG} can be reproduced by the classical action of the field theory of QH edges:

$$S_{QH} = \int d^2x \left(N(x)\frac{\Lambda^2}{4} + \frac{1}{N}\left((\partial_x\varphi)^2 + \frac{1}{\ell_B^2} \right) \right), \quad (67)$$

where $N(x)$ is a lapse function. When we take $N(x) = 1$, S_{QH} yields the action of the quantum field theory for the edges. By taking the variation of S_{QH} with respect to $N(x)$, we get

$$N(x) = \frac{2}{\Lambda\ell_B} \sqrt{1 + \ell_B^2(\partial_x\varphi)^2}. \quad (68)$$

It turns out that substitution of the above $N(x)$ into S_{QH} reproduces the value of S_{QG} in (66). Though the correct relation between the theories with S_{QG} and S_{QH} remains vague at present, it may be interesting to explore the correspondence and quantum gravity effective theory for the QH edges. In this case, the circular edge corresponds to a closed universe. The interpretation of the wave functions of the quantum closed universe, which satisfy the Wheeler-DeWitt equation, can be developed from the viewpoint of the many-body wave functions of the QH systems. As a last comment it is worth mentioning that subtle effects of quantum gravity, which are predicted by recent holographic framework based on DS/dS correspondence [27–31] closely related to the subject of information loss paradox in black holes, might yield different results in entanglement calculation from our results based on quantum field theory in fixed curved spacetime background. Though the analysis based on the holographic treatment is out of the scope of this paper, this direction of investigation will reveal the feature of quantum gravity and we hope the future QH experiments will be capable of discriminating which theories are suitable to effectively describe the detected behavior of entanglement.

APPENDIX A: DERIVATION OF COORDINATE TRANSFORMATION

We review coordinate transformation in [12]. The metric is

region I : $L/2 \leq x_I$, $\quad ds^2 = -dx_I^+ dx_I^-$

region II : $-L/2 \leq x \leq L/2$, $\quad ds^2 = -e^{2\Theta(t)} dx^+ dx^-$

region III : $x_{III} \leq -L/2$, $\quad ds^2 = -dx_{III}^+ dx_{III}^-$,

where $e^{\Theta(t)}$ is the scale factor in region II. We consider the coordinate transformation of the form $x^+ = x^+[x_{I,III}^+]$, $x^- = x^-[x_{I,III}^-]$, which keeps conformal invariance.

1. Regions II and III

We look for coordinates $x_{III}^+[x^+], x_{III}^-[x^-]$ which cover regions II and III. The matching point is $x^1 = x_{III}^1 = (x_{III}^+ - x_{III}^-)/2 = -L/2$. The matching condition is

$$x_{III}^+[t - L/2] - x_{III}^-[t + L/2] = -L. \tag{A1}$$

By taking the derivative with respect to t, we obtain

$$\frac{dx_{III}^+}{dx^+}[t - L/2] = \frac{dx_{III}^-}{dx^-}[t + L/2]. \tag{A2}$$

The matching of the metric between region II and III (at $x = x_{III} = -L/2$) is

$$e^{2\Theta(t)} \frac{dx^+}{dx_{III}^+} \frac{dx^-}{dx_{III}^-} = 1 \quad \therefore \quad \frac{dx_{III}^+}{dx^+}[t - L/2] = e^{\Theta(t)}. \tag{A3}$$

By shifting the argument of the functions,

$$\frac{dx_{III}^+}{dx^+}[x^+] = e^{\Theta(x^+ + L/2)}, \tag{A4}$$

and we obtain

$$\begin{aligned} x_{III}^+[x^+] &= \int_0^{x^+} dy e^{\Theta(y + L/2)} \\ &= \int_{L/2}^{x^+ + L/2} dy e^{\Theta(y)} \\ &= \Phi[x^+ + L/2] - \Phi[L/2], \end{aligned} \tag{A5}$$

where we have fixed the integration constant such that $x_{III}^+ \propto x^+$ for constant Θ and the function Φ is introduced by

$$\Phi[x] = \int_0^x dy e^{\Theta(y)}. \tag{A6}$$

The coordinate function $x_{III}^-(x^-)$ can be derived from (A1) as

$$\begin{aligned} x_{III}^-[x^-] &= x_{III}^+[x^- - L] + L \\ &= \int_0^{x^- - L} dy e^{\Theta(y + L/2)} + L \\ &= \Phi[x^- - L/2] - \Phi[L/2] + L. \end{aligned} \tag{A7}$$

From (A5) and (A7),

$$dx_{III}^+ dx_{III}^- = e^{\Theta(x^+ + L/2)} e^{\Theta(x^- - L/2)} dx^+ dx^-, \tag{A8}$$

and the metric in region II can be written as

$$\begin{aligned} ds_{II}^2 &= -e^{2\Theta(t)} dx^+ dx^- \\ &= -\exp[2\Theta(t) - \Theta(x^+ + L/2) - \Theta(x^- - L/2)] dx_{III}^+ dx_{III}^-. \end{aligned} \tag{A9}$$

At the boundary $x^1 = -L/2$, $x^+ = t - L/2$ and $x^- = t + L/2$. Thus, the metric becomes the flat form $ds_{II}^2 = -dx_{III}^+ dx_{III}^-$, and can be extended to the flat region III using coordinates $x_{III}^\pm$.

2. Regions I and II

The condition of the matching at $x^1 = L/2$ yields

$$x_I^+[t + L/2] - x_I^-[t - L/2] = L. \tag{A10}$$

The coordinate function is

$$x_I^+[x^+] = \int_0^{x^+} dy e^{\Theta(y - L/2)} = \Phi[x^+ - L/2] - \Phi[-L/2]. \tag{A11}$$

In a similar way, we obtain

$$\begin{aligned} x_I^-[x^-] &= x_I^+[x^- + L] - L \\ &= \int_0^{x^- + L} dy e^{\Theta(y - L/2)} - L \\ &= \Phi[x^- + L/2] - \Phi[-L/2] - L. \end{aligned} \tag{A12}$$

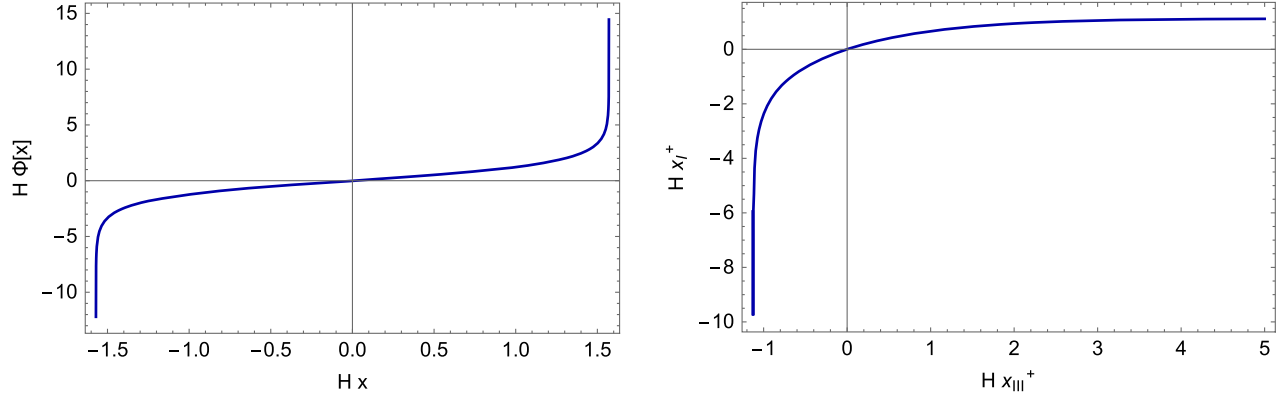From (A11) and (A12),

$$dx_I^+ dx_I^- = e^{\Theta(x^+ - L/2)} e^{\Theta(x^- + L/2)} dx^+ dx^-, \tag{A13}$$

and the metric in region II becomes

$$\begin{aligned} ds_{II}^2 &= -e^{2\Theta(t)} dx^+ dx^- \\ &= -\exp[2\Theta(t) - \Theta(x^+ - L/2) - \Theta(x^- + L/2)] dx_I^+ dx_I^-. \end{aligned} \tag{A14}$$

At the boundary $x^1 = L/2$, $x^+ = t + L/2$ and $x^- = t - L/2$. Thus, the metric becomes the flat form $ds_{II}^2 = -dx_I^+ dx_I^-$,

FIG. 12. The function $\Phi(x)$ and $x_I^+ = f(x_{III}^+)$.

and can be extended to the flat region III using coordinates $x_I^\pm$.

3. Relation between x_I and x_{III}

Using the function Φ,

$$x_{III}^+ = \Phi(y^+ + L/2) - \Phi(L/2),$$
$$x_I^+ = \Phi(y^+ - L/2) - \Phi(-L/2), \quad (A15)$$

$$x_{III}^- = \Phi(y^- - L/2) - \Phi(L/2) + L,$$
$$x_I^- = \Phi(y^- + L/2) - \Phi(-L/2) - L. \quad (A16)$$

By eliminating $y^\pm$, we obtain a connection formula between x_I and x_{III}:

$$x_I^+ = \Phi[-L + \Phi^{-1}[x_{III}^+ + \Phi[L/2]]] - \Phi[-L/2] =: f(x_{III}^+),$$
$$(A17)$$

$$x_{III}^- = \Phi[-L + \Phi^{-1}[x_I^- + L + \Phi[-L/2]]] - \Phi[L/2] + L.$$
$$(A18)$$

APPENDIX B: DE SITTER CASE: GLOBAL CHART

We consider the global de Sitter spacetime. The conformal factor is given by

$$e^{\Theta(t)} = \frac{1}{\cos(Ht)}, \quad (B1)$$

and the function Φ is Fig. 12

$$\Phi(x) = \int_0^x dy\, e^{\Theta(y)} = \frac{1}{2H} \ln \frac{1 + \sin Hx}{1 - \sin Hx},$$

$$\Phi^{-1}(x) = \frac{1}{H} \arcsin \tanh Hx. \quad (B2)$$

For $\pi/4 < LH < \pi/2$, from the behavior of the function x_I^+, we can obtain the global structure as shown in Fig. 13. Figure 14 shows a wave form of $\exp(-ikf(x_{III}^+))$. As x_{III} approaches a finite negative value, the wavelength becomes zero, which reflects a blueshift of waves by the past horizon $\mathscr{H}^-$. On the other hand, for a large value of x_{III}^+, the wavelength becomes infinite which reflects a redshift of waves by the future horizon $\mathscr{H}^+$.
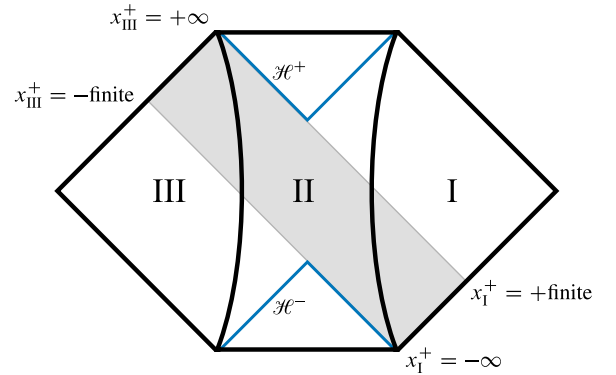
FIG. 13. Penrose diagram for the global de Sitter case with $\pi/4 < LH < \pi/2$.
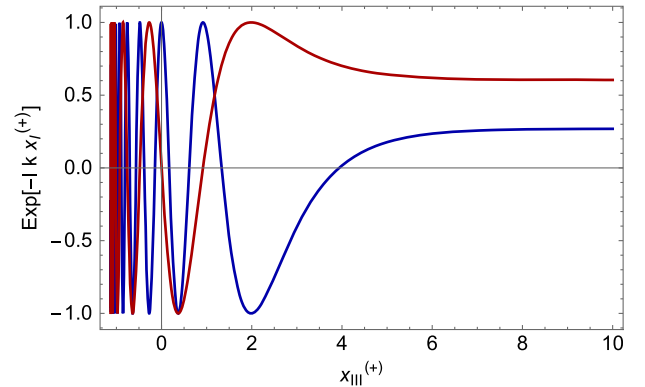
FIG. 14. Wave form of $\exp(-ikf(x_{III}^+))$. The real part (blue) and the imaginary part (red) of the wave are shown.

[1] C. Barceló, S. Liberati, and M. Visser, Analogue gravity, Living Rev. Relativity **8,** 12 (2005).

[2] J. Steinhauer, Observation of quantum Hawking radiation and its entanglement in an analogue black hole, Nat. Phys. **12,** 959 (2016).

[3] J. R. Muñoz de Nova, K. Golubkov, V. I. Kolobov, and J. Steinhauer, Observation of thermal Hawking radiation and its temperature in an analogue black hole, Nature (London) **569,** 688 (2019).

[4] S. S. Hegde, V. Subramanyan, B. Bradlyn, and S. Vishveshwara, Quasinormal Modes and the Hawking-Unruh Effect in Quantum Hall Systems: Lessons from Black Hole Phenomena, Phys. Rev. Lett. **123,** 156802 (2019).

[5] S. Dalui, B. R. Majhi, and P. Mishra, Horizon induces instability locally and creates quantum thermality, Phys. Rev. D **102,** 044006 (2020).

[6] V. Subramanyan, S. S. Hegde, S. Vishveshwara, and B. Bradlyn, Physics of the inverted harmonic oscillator: From the lowest Landau level to event horizons, Ann. Phys. (Amsterdam) **435,** 168470 (2021).

[7] D. Yoshioka, *The Quantum Hall Effect* (Springer-Verlag, New York, 2002).

[8] D. Tong, Lectures on the quantum Hall effect, arXiv:1606 .06687.

[9] M. Hotta, J. Matsumoto, and G. Yusa, Quantum energy teleportation without a limit of distance, Phys. Rev. A **89,** 012311 (2014).

[10] A. Kamiyama, M. Matsuura, J. N. Moore, T. Mano, N. Shibata, and G. Yusa, Real-time and space visualization of excitations of the $\nu = 1/3$ fractional quantum Hall edge, Phys. Rev. Res. **4,** L012040 (2022).

[11] A. Kamiyama, M. Matsuura, J. N. Moore, T. Mano, N. Shibata, and G. Yusa, Dynamics of the fractional quantum Hall edge probed by stroboscope measurements of trions, arXiv:2212.05507.

[12] M. Hotta, Y. Nambu, Y. Sugiyama, K. Yamamoto, and G. Yusa, Expanding edges of quantum Hall systems in a cosmology language: Hawking radiation from de Sitter horizon in edge modes, Phys. Rev. D **105,** 105009 (2022).

[13] Y. Nambu, Entanglement of quantum fluctuations in the inflationary universe, Phys. Rev. D **78,** 044023 (2008).

[14] Y. Nambu and Y. Ohsumi, Classical and quantum correlations of scalar field in the inflationary universe, Phys. Rev. D **84,** 044028 (2011).

[15] A. Matsumura and Y. Nambu, Large scale quantum entanglement in de Sitter spacetime, Phys. Rev. D **98,** 025004 (2018).

[16] A. Peres, Separability Criterion for Density Matrices, Phys. Rev. Lett. **77,** 1413 (1996).

[17] P. Horodecki, Separability criterion and inseparable mixed states with positive partial transposition, Phys. Lett. A **232,** 333 (1997).

[18] R. Simon, Peres-Horodecki Separability Criterion for Continuous Variable Systems, Phys. Rev. Lett. **84,** 2726 (2000).

[19] G. Vidal and R. Werner, Computable measure of entanglement, Phys. Rev. A **65,** 032314 (2002).

[20] M. B. Plenio, Logarithmic Negativity: A Full Entanglement Monotone That is Not Convex, Phys. Rev. Lett. **95,** 090503 (2005).

[21] T. Hiroshima, G. Adesso, and F. Illuminati, Monogamy Inequality for Distributed Gaussian Entanglement, Phys. Rev. Lett. **98,** 050503 (2007).

[22] A. Holevo and R. Werner, Evaluating capacities of bosonic Gaussian channels, Phys. Rev. A **63,** (2001) 032312.

[23] L. Bombelli, R. Koul, J. Lee, and R. Sorkin, Quantum source of entropy for black holes, Phys. Rev. D **34,** 373 (1986).

[24] M. Srednicki, Entropy and Area, Phys. Rev. Lett. **71,** 666 (1993).

[25] I. Bengtsson and K. Zyczkowski, A brief introduction to multipartite entanglement, arXiv:1612.07747.

[26] C. Emary, N. Lambert, and F. Nori, Corrigendum: Leggett-Garg inequalities, Rep. Prog. Phys. **77,** 039501 (2014).

[27] G. Geng, S. Grieninger, and A. Karch, Entropy, entanglement and swampland bounds in DS/dS, J. High Energy Phys. 06 (2019) 105.

[28] G. Geng, Some information theoretic aspects of de-Sitter holography, J. High Energy Phys. 02 (2020) 005.

[29] G. Geng, Non-local entanglement and fast scrambling in de-Sitter holography, Ann. Phys. (Amsterdam) **426,** 168402 (2021).

[30] G. Geng, Y. Nomura, and H-Y. Sun, Information paradox and its resolution in de Sitter holograph, Phys. Rev. D **103,** 126004 (2021).

[31] S. Raju, Lessons from the information paradox, Phys. Rep. **943,** 1 (2022).